Diffusion de l’hydrogène d’un liquide kimberlitique à la forstérite

L’hydrogène est un élément présentant des taux de diffusions élevés dans l’olivine à haute température (e.g. Demouchy et al., 2006; Demouchy and Mackwell, 2006), et ayant un impact significatif sur les propriétés physiques et chimiques du manteau (Demouchy et al., 2012; Gaetani and Grove, 1998; Hirth and Kohlstedt, 1996; Jacobsen et al., 2008; Karato, 1990; Mackwell et al., 1985). La connaissance de son impact sur la rhéologie du manteau a ainsi conduit des géologues à suggérer que de faibles teneurs en hydrogène pouvaient avoir généré un contraste de viscosité suffisant pour préserver le craton de la convection mantellique et de la tectonique des plaques durant plusieurs milliards d’années (Doin et al., 1997 ; Pollack, 1986). Pourtant, les analyses par spectroscopie infrarouge à transformée de Fourrier (IRTF) révèlent des teneurs en hydrogène élevées dans l’olivine des péridotites du Kaapvaal jusqu’à une profondeur de 150 km (Baptiste et al., 2012; Peslier et al., 2010). De telles teneurs pourraient avoir été héritées à la suite d’un épisode métasomatique et donc être représentatives de la composition de la racine cratonique en profondeur, mais la possibilité d’une contamination durant extraction par les kimberlites riches en volatiles ne peut être exclue malgré l’absence de profils de diffusion (Baptiste et al., 2012). Toutefois, aucune étude expérimentale n’a à ce jour testé ou quantifié la diffusion en hydrogène entre un liquide kimberlitique et l’olivine, nous empêchant de conclure sur l’origine exacte des teneurs en hydrogène élevées dans l’olivine dans notre étude sur les xénolites du Kaapvaal.

Le travail expérimental présenté dans ce chapitre avait donc pour objectif de tester si l’incorporation d’hydrogène par diffusion ionique pouvait avoir lieu entre un liquide kimberlitique et la forstérite à haute pression et température. Il repose sur 5 expériences au piston cylindre effectuées au laboratoire Magmas et Volcans de l’Université de Clermont-Ferrand à 1200-1300°C et 1 GPa, pour des durées de 1 min, 5h et 23h.

Les analyses de deux capsules par EBSD (Electron Back-Scattered Diffraction) et microsonde électronique montrent qu’après 5h et 23h d’expérience, une surcroissance du cristal de forstérite, possédant la même orientation cristallographique a cristallisée. Le liquide a cristallisé ailleurs sous la forme de cristaux micrométriques de forstérite automorphes aux orientations cristallographiques aléatoires, ainsi que sous la forme de cristaux nanométriques d’une phase alumineuse et d’une phase calcique. Les analyses des teneurs en hydrogène par spectroscopie IRTF après expérience révèlent qu’aucun des cristaux de forstérite ne présente de signe d’hydratation, et ce, malgré la saturation en H_2O du système et des durées d’expérience longues. La présence de CO_2 dans le système pourrait ainsi avoir abaissé la fugacité en H_2O au point de ne pouvoir hydrater ni le cristal de forstérite, ni sa surcroissance.

De tels résultats suggèrent que les teneurs en hydrogène élevées dans les xénolites mantelliques du craton du Kaapvaal ont été acquises durant un épisode métasomatique plutôt que durant leur transport à la surface par les kimberlites, et sont certainement représentatives de la composition en profondeur de la racine cratonique.

Inhibition of forsterite hydration from CO_2-H_2O-rich kimberlitic liquid

Virginie Baptiste[1*], Sylvie Demouchy[1], Shantanu Keshav[1], Fleurice Parat[1], Nathalie Bolfan-Casanova[2] & Pierre Condamine[2]

[1]Géosciences Montpellier, Université Montpellier 2 & CNRS, CC 60, Place E. Bataillon, 34095 Montpellier cedex 5, France.
[2] Laboratoire Magmas et Volcans, CNRS, 5, rue Kessler, 63000 Clermont-Ferrand, France

Running title: Inhibition of forsterite hydration from CO_2-H_2O-rich kimberlitic liquid

(*) corresponding author: virginie.baptiste@gm.univ-montp2.fr;
Phone: +33 467144912
Fax: +33 467143603

Abstract

Knowledge of the high diffusivity of hydrogen has raised the question of the origin and relevance of high OH concentrations measured in mantle xenoliths transported by volatile-rich magmas. To test if hydrogen incorporation by ionic diffusion can occur between a volatile-rich kimberlitic liquid and forsterite at high pressure and temperature, we conducted high pressure experiments using a piston-cylinder apparatus at 1200-1300°C and 1 GPa for durations of 1 min, 5h, and 23h. Kimberlitic liquid in the system CaO-MgO-Al_2O_3-SiO_2-CO_2-H_2O and synthetic forsterite single crystals were chosen as a first simplification of the complex natural kimberlite composition. Unpolarized Fourier transform infrared spectroscopy was used to quantify OH concentrations in the crystallographically oriented forsterite. Electron backscattered diffraction and electron microprobe analysis were performed to identify the run products. After 5h and 23h, a forsterite overgrowth crystallized with the same orientation as the initial forsterite single crystal. The kimberlitic liquid has crystallized as micron-scale euhedral forsterite neocrystals with random crystallographic orientations, as well as a nano-scale aluminous phase and a calcic phase. Despite water-saturation of the system and long duration, none of the initial forsterite single crystals display signs of hydration such as hydrogen diffusion profile from the border toward the center of the crystal. The presence of CO_2 in the system may have lowered the H_2O fugacity to such extends which has prohibiting meaningful hydration of the forsterite single crystal or its overgrowth. These experimental results favor a deep mantle origin of the high OH content found in natural mantle-derived xenoliths transported in kimberlites, as reported from the Kaapvaal craton. It also points out to the fact that hydration must take place in a CO_2-poor environment.

Keywords: Kimberlite, water, hydrogen, diffusion, olivine, point defect.

Introduction

Incorporation of hydrogen in nominally anhydrous minerals (NAMs), even at trace concentrations (ppm by weight level), is known to have a significant impact on the chemical and physical properties of the rocks and minerals in Earth's mantle such as melting temperature, electrical conductivity, seismic velocities, and rheology (e.g., Karato et al., 1990; Mackwell et al., 1985; Hirth and Kohlstedt, 1996; Demouchy et al., 2012; Gaetani and Grove, 1998; Jacobsen et al., 2008). For instance, in terms of rheology, olivine controls the viscosity of the lithosphere root and its low OH^- concentrations (< 20 ppm H_2O wt based on FTIR calibration from Paterson, 1982) was proposed to increase the mantle viscosity and hence a strongly OH-depleted zone at the base of the craton root could be responsible for the longevity of the South African craton (Peslier et al., 2010; Baptiste et al., 2012). This hypothesis was tested recently by studying mantle peridotites from the Siberian craton, but was not confirmed (Doucet et al., 2014). Prior to these recent studies, several publications have reported high OH concentrations (> 30 ppm H_2O wt) in olivine from mantle xenoliths, olivine megacrysts, and kimberlitic olivine phenocrysts from several cratons (e.g., South Africa, Siberia, and Canada; see Miller et al., 1987; Matsyuk et al., 1998; Bell et al., 2004; Matsyuk and Langer, 2004; Peslier et al., 2010; Peslier, 2010, Doucet et al., 2014). In particular, relatively high OH concentrations in olivine (up to 150 ppm H_2O wt) have been reported in olivine of mantle xenoliths from the Kaapvaal craton (Peslier et al., 2010; Baptiste et al., 2012), except for the deepest and infrequent samples, which are almost dry (<10 ppm H_2O wt). Further, high OH concentrations in olivine (54-419 ppm H_2O wt) have been measured in megacrysts and macrocrysts from kimberlites (Bell et al., 2004, Matsyuk and Langer, 2004; Matveev and Stachel, 2007) suggesting that kimberlite would be a favorable environment for hydrogen incorporation in olivine.

Moreover, studies on Kaapvaal mantle xenoliths usually report homogeneous OH concentration profiles across olivine grains suggesting the absence of hydration or dehydration process caught-in-the-act (Peslier et al., 2010; Baptiste et al., 2012). However, the origin of hydrogen in olivines from the cratonic mantle still remains unclear. High OH contents in olivine in Kaapvaal xenoliths could have been inherited from (1) metasomatism, if water-saturated fluids or water-saturated percolating melts impregnated the cratonic root, or (2) during transport by the water-rich kimberlitic magmas (Brooker et al., 2011; Baptiste et al., 2012). Yet, so far, experimental studies have not tested the second hypothesis or quantified the diffusion of hydrogen between a volatile-rich kimberlitic melt/magma and olivine.

The aim of this study is to test if hydrogen incorporation by ionic diffusion can occur between a model very volatile-rich kimberlitic liquid in the system CaO-MgO-Al_2O_3-SiO_2-CO_2-H_2O (CMAS-CO_2-H_2O) and iron-free forsterite at high pressure and temperature during transport toward the surface.

Sample preparation and experimental method

A synthetic volatile-rich kimberlite starting material was prepared with high purity oxides (SiO_2 - Aldrich, 99.995%, Al_2O_3 - Alfa Aesar, 99.998%, MgO - Alfa Aesar, 99.998%,), high purity calcium carbonate ($CaCO_3$ - Alfa Aesar, 99.998%), magnesium hydroxide (brucite, $Mg(OH)_2$ - Alfa Aesar, 99.998%), and a very pure natural magnesite ($MgCO_3$) from Oberdorf (Austria, see Buob et al., 2006). The silicate portion of the starting mixture was prepared first. The components MgO, Al_2O_3, and SiO_2 were fired in platinum (Pt) crucibles for at least 18-20 hours in air at 1250^{o}C, and $CaCO_3$ at 400^{o}C. Pt crucibles were used that had not been previously utilized to dry either iron metal or iron oxides. Afterwards, the fired oxides and $CaCO_3$ were immediately mixed in appropriate proportions, and ground for at least 1 hour under ethanol in an agate mortar. After drying under an infrared (IR) heat lamp, the mixture was decarbonated in air in a high temperature, room pressure furnace. To decarbonate, the temperature of the furnace was slowly ramped to 1000^{o}C over 10 hours, and maintained at this temperature for 6-7 hours. After this step, the mixture was taken out of the furnace, and then transferred to another high temperature furnace to prepare a glass by melting the mixture in air at 1650^{o}C for about 4 hours. To quench this liquid to a glass, the Pt-crucible containing the mixture was partially immersed in an ice-water bath, and the resulting glass was optically clear and transparent. This glass was finely ground under ethanol for about 30-40 minutes, and using the same procedure, glassing was repeated twice more. To ensure homogeneity, the silicate glass was then re-ground for 1 hour under ethanol in an agate mortar, and then dried under an IR heat lamp for about 1 hour. Finally, CO_2 and H_2O were added in the silicate glass as magnesite and brucite, respectively. Ground magnesite and brucite were fired at 250°C and 120°C, respectively in air in a Pt-crucible for over 17 hours, to obtain stochiometric components, then mixed and ground with the silicate glass in an agate mortar under ethanol for another 1 hour. The final powder was stored in a desiccator.

Table 1: Forsterite and starting material composition, average kimberlite group-I and group-II compositions, and compositions of run products from VB12.

Wt.%	**Starting composition**	**Group I Kimberlite Average***	**Group II Kimberlite Average***	**Forsterite crystal composition**	**VB12 compositions (after run)**				
					Fo single crystal	Fo overgrowth	Fo neocrystals	Al-rich phase	Ca-rich phase
SiO_2	30	26.15	33.89	44.76	43.25	43.02	43.08	4.73	28.35
TiO_2	0	2.58	1.77	0.00	0.01	0.00	0.00	0.00	0.03
Al_2O_3	4	2.76	3.76	-0.01	-0.02	0.46	1.21	53.37	1.78
FeO		-	-	0.00	-0.01	0.00	0.00	0.16	0.05
Fe_2O_3	0	10.72	8.76	-	-	-	-	-	-
MnO	0	0.19	0.18	0.00	0.01	0.00	0.00	0.00	0.01
MgO	28	25.20	23.15	55.41	56.49	54.61	54.99	25.04	18.86
CaO	14	13.20	9.96	0.00	0.00	0.43	0.31	10.20	28.75
Na_2O	0	0.16	0.25	-0.01	0.00	0.00	0.00	0.01	0.02
K_2O	0	0.83	3.63	0.00	0.00	0.00	0.00	0.01	0.00
P_2O_5	0	2.04	1.85	-	-	-	-	-	-
SO_3	0	0.17	0.21	-	-	-	-	-	-
NiO	0	0.11	0.14	0.00	0.01	0.00	0.00	0.01	0.00
Cr_2O_3	0	0.18	0.23	-0.01	0.00	0.00	0.00	0.00	0.00
LOI	-	14.71	10.75	-	-	-	-	-	-
H_2O-	-	0.27	1.34	-	-	-	-	-	-
H_2O+	-	6.67	7.33	-	-	-	-	-	-
H_2O	13	-	-	-	-	-	-	-	-
CO_2	11	8.19	4.21	-	-	-	-	-	-
total		84.29	87.78	100.16	99.78	98.51	99.60	93.53	77.85

* Average compositions from Becker and Le Roex (2006).

Fo:single crystal of crystallographically oriented forsterite

The composition of this starting composition is reported in Table 1 and was synthetized on the basis of published compositions of: (1) erupted kimberlites (Smith et al., 1985a, b; Mitchell, 1986, 1995; Becker and Le Roex, 2006; Kamenetsky et al., 2008; Kjarsgaard et al., 2009; Sparks et al., 2009, Brooker et al., 2011), (2) the results of experimental petrology of kimberlites in the system CMAS-CO_2 (Dalton and Presnall, 1998; Gudfinnsson and Presnall, 2005), and (3) the solubility of water (H_2O) in model carbonatitic melts (Keppler, 2003). From studies in the system CMAS-CO_2 (e.g., Gudfinnsson and Presnall, 2005), it appears that kimberlites are not stable liquids at 1 GPa, but at higher pressures, >5 GPa. At such high pressures, the liquid used here will be in equilibrium with forsterite, orthopyroxene (opx), clinopyroxene (cpx), and garnet. Here, the starting composition was chosen to target hydration of olivine from kimberlite liquid during transport toward the surface (e.g., then in a rising metastable kimberlitic liquid), and accordingly, the experiment were run at a lower pressure than their estimated depth of genesis, on the basis of previous experimental petrology studies (Dalton and Presnall, 1998; Gudfinnsson and Presnall, 2005).

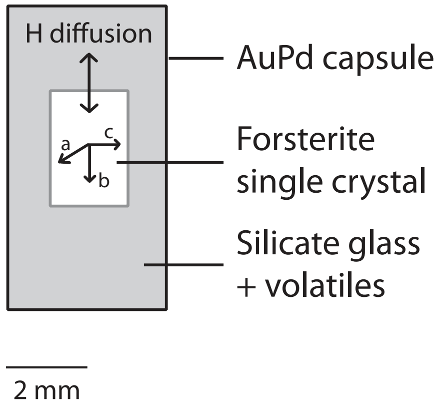

Figure 1: Schematic illustration of the capsule assembly for high pressure diffusion experiments.

High pressure assemblies were prepared by placing a crystallographically oriented single crystal of forsterite (iron-free forsterite from Roditi) within ~60 mg of starting material, in 4 mm outer diameter and 7 mm length gold-palladium ($Au_{75}Pd_{25}$) capsules (see Figure 1), which were then welded shut. AuPd capsules were chosen to minimize water loss. Single crystals of forsterite were in average 2.20 × 2.65 × 1.9 mm (for [100], [010], and [001] being the crystallographic axes, respectively). The capsules were then placed in salt (NaCl) cylinders. Experiments were performed in a 19.1 mm non end-loaded piston cylinder apparatus (pressure calibrations detailed in Xirouchakis et al., 2001). Temperature was controlled using a $W_{74}Re_{26}$-$W_{95}Re_5$ thermocouple. Five runs were completed, and all cells were pressurized to 1.0 GPa. They were annealed at 1200°C for 1 min, 5h and 23h, or annealed at 1250 and 1300°C for 5h. Annealing duration over 2 hours at temperature above 900 °C is long enough to permit detectable hydrogenation of olivine or forsterite (Demouchy and Mackwell, 2003, 2006) at pressures above 0.2 GPa. Temperature quench rate was 50 $°C.s^{-1}$. Experimental conditions are summarized in Table 2. Short duration experiments were chosen to avoid significant hydrogen loss or reaction with the capsule (<50h). The experimental duration of 1 min was chosen to test if the heating up stage allows any significant hydrogen diffusion between the forsterite crystal from the volatile-rich kimberlite melt. All the experiments reported here were performed at Laboratoire Magmas et Volcans, Clermont-Ferrand (France).

Table 2: Experimental conditions in piston-cylinder.

Run	Sample	Pressure (GPa)	Temperature (°C)	Duration (min)	free fluid
1	VB7	1.0	1200	1	✓
2	VB1	1.0	1200	300	✓
3	VB6	1.0	1200	1380	✓
4	VB10	1.0	1300	300	✓
5	VB12	1.0	1250	300	✓

Sample analysis

Electron microprobe analysis (EMPA)

Major elements composition of the forsterite crystals was analyzed before experiments using a Cameca SX100 electron microprobe at Microsonde Sud facility, in Montpellier (France). Analytical conditions were a focused beam of 20 kV of accelerating voltage and 10 nA probe current at the Faraday cup. After experimental runs, the composition of the forsterite crystal and the newly formed phases was also analyzed. Results are reported in Table 1. Typical composition of natural Group-I and Group-II kimberlites from Becker and LeRoex (2006) are also provided for comparison. After experimental runs, each capsule was pierced to check for excess free fluid to insure water saturation of the liquid; each capsule has shown fluid bubbles.

Fourier transform infrared spectroscopy

Each capsule was doubly hand-polished for unpolarized *Fourier transform infrared spectroscopy (*FTIR) analysis. The sections were immersed in pure acetone for at least 12h to dissolve any intergranular CrystalBond glue before analysis. FTIR spectroscopy analyses were made at the Laboratoire des Colloïdes, Verres, Nanomatériaux in Montpellier (France) using a Bruker IFS66v coupled with a Bruker HYPERION microscope and a liquid nitrogen-cooled mercury-cadmium-telluride (MCT) detector. A Globar light source and a Ge-KBr beam splitter were used to generate unpolarized mid-infrared radiation. A background measurement was performed before analysis. Measurements were made with aperture sizes between 30 to 100 µm, with the IR beam parallels to [010] crystallographic axis of the forsterite crystals (i.e., across the basal plane of the capsule). Two hundred scans were accumulated with a resolution of 4 cm^{-1} for each measurement. A baseline correction was applied on each spectrum using the OPUS software. Spectra were then normalized to a sample thickness of 1 cm. Fractures and inclusions were strictly avoided. The sample thickness was measured using a micrometer with an accuracy of ± 1 µm. The calibration of Paterson (1982) was used to quantify the OH concentration in each mineral phase:

$$C_{OH} = \frac{X_i}{150\zeta} \int \frac{k(\bar{v})}{(3780 - \bar{v})} d\bar{v}$$

where C_{OH} is the hydroxyl concentration (in mol H/l), ζ is an orientation factor (1/3 for unpolarized measurements), and $k(\bar{v})$ is the absorption coefficient in cm^{-1} for a given wavenumber $\bar{v}$. Xi is a density factor equal to 2750 ppm H_2O wt, for iron-free forsterite (see Bolfan-Casanova et al., 2000, for the calculation method).

Electron-backscattered diffraction

After experimental runs, sections cut through VB6 and VB12 capsules were mounted on epoxy plugs and carefully polished. Analyses were performed with a Scanning electron microscope (SEM) CamScan X500FE CrystalProbe equipped with an Electron-backscattered diffractometer (EBSD) at Geosciences Montpellier (France), using an acceleration voltage of 25kV and a working distance of 20 mm. To avoid charging of the samples, low vacuum conditions were chosen (5 Pa of gaseous nitrogen). EBSD patterns were produced by interaction between an electron beam at 20° to the horizontal sample stage (see Demouchy et al. 2011 for a detailed description of the CrystalProbe-EBSD). Data were acquired using CHANNEL5 software. Punctual measurements were made to determine the crystallographic orientation of the forsterite single crystals and the newly produced crystalline phases.

Results

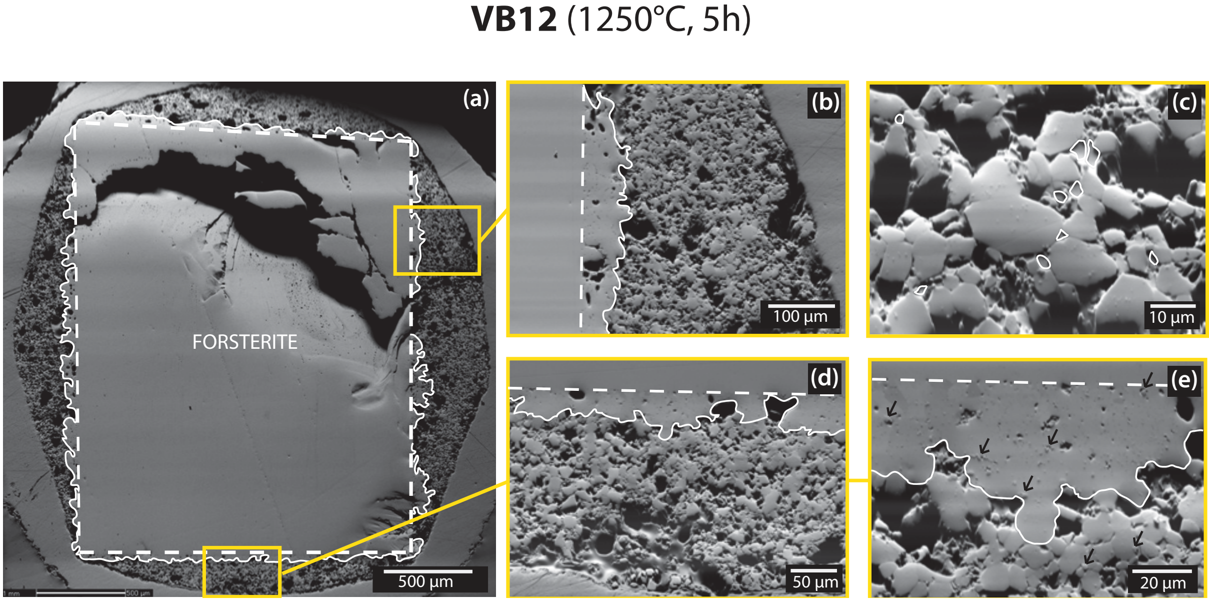
VB12 (1250°C, 5h)

Figure 2: SEM-images of VB12 after experiment, showing (a) the entire capsule section with the forsterite single crystal displaying a well-defined overgrowth, (b) and (d) the forsterite single crystal boundary, its overgrowth, and the surrounding euhedral forsterites, (c) the euhedral forsterite and the Ca-rich phase are circled by a white line, (e) Al-rich phase within the forsterite overgrowth and close to euhedral forsterites.

Results from SEM-EBSD will be presented first, followed by the characterization by EMPA and finally FTIR results. SEM images of the typical recovered capsule are shown in Figure 2. During the experiments, the original shape of the forsterite single crystal has been well preserved, despite few fractures due to decompression. Micrometer-size forsterite overgrowths which have formed, display the same crystallographic orientation (homo-epitaxy) as the initial forsterite single crystal as shown by the Kikuchi bands pattern in Figures 3a and 3b. The width of the forsterite overgrowth increases with increasing run duration and reaches up to 135 microns after 23h. In addition, the kimberlitic melt has crystallized euhedral neocrystals of forsterite with variable crystallographic orientations as shown in Figures. 2c and 3. From EBSD and Energy Dispersive X-ray (EDX), a minor spinel-like (cubic) Al-rich crystalline phase was also identified, occurring mostly as small crystallites (tens of nanometers) within the forsterite overgrowth as shown in Figures. 2e, and by point analysis in Figures. 3d. A Ca-rich phase with well-defined crystallographic planes has also been identified (Figures. 2, and 3e). Several vesicles were present (20 μm in diameter), but no quenched vitrified melt was observed.

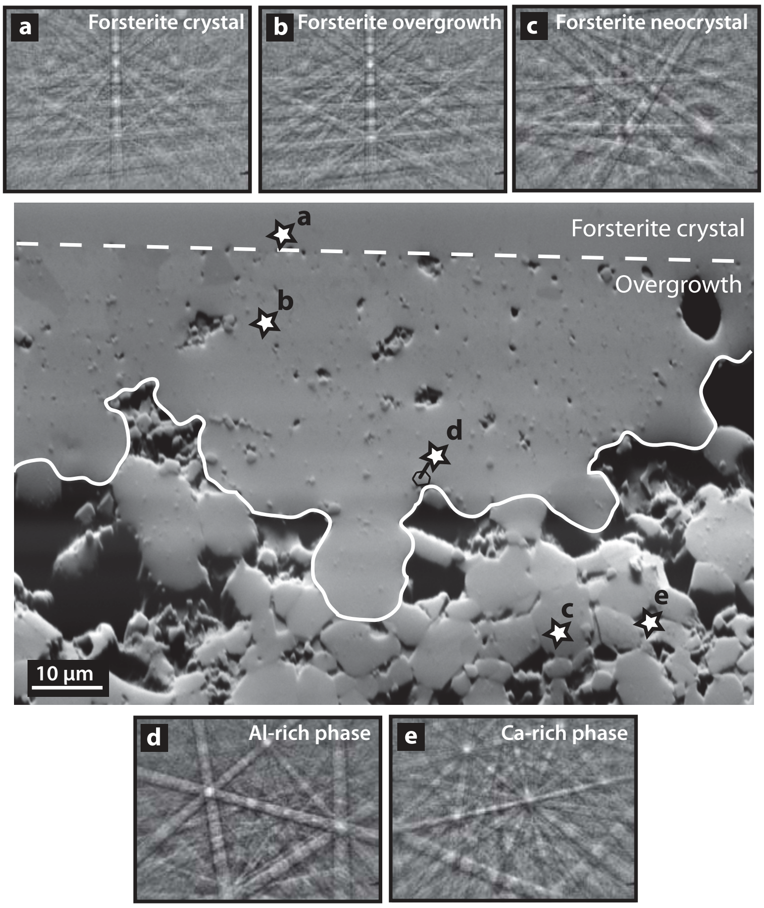

Figure 3: SEM-images of VB12 and electron back-scattered diffraction patterns (Kikuchi's bands: Kikuchi, 1928) of (a) the forsterite single crystal, (b) the forsterite overgrowth, (c) a euhedral forsterite, (d) the Al-rich spinel, (e) the Ca-rich phase.

Subsequently, EMPA analyses after EBSD reported in Table 1 reveal that the forsterite single crystal, forsterite overgrowths, and the forsterite neocrystals have very similar major element composition. The Al-rich phase has a composition closer to spinel than sapphirine and corundum (Ackermand et al., 1975), but is enriched in CaO (>10 wt.%). The Ca-rich phase has a composition close to monticellite ($CaMgSiO_4$, Deer et al., 1992, p354-355; Brooker et al., 2011) but with lower silica content, it could be a carbonate-like phase as well. For both the Al-rich and Ca-rich phases, the size of the phase (below 10 nanometer) has significantly limited the outcomes and quality of the EMPA analyses and thus their identification.

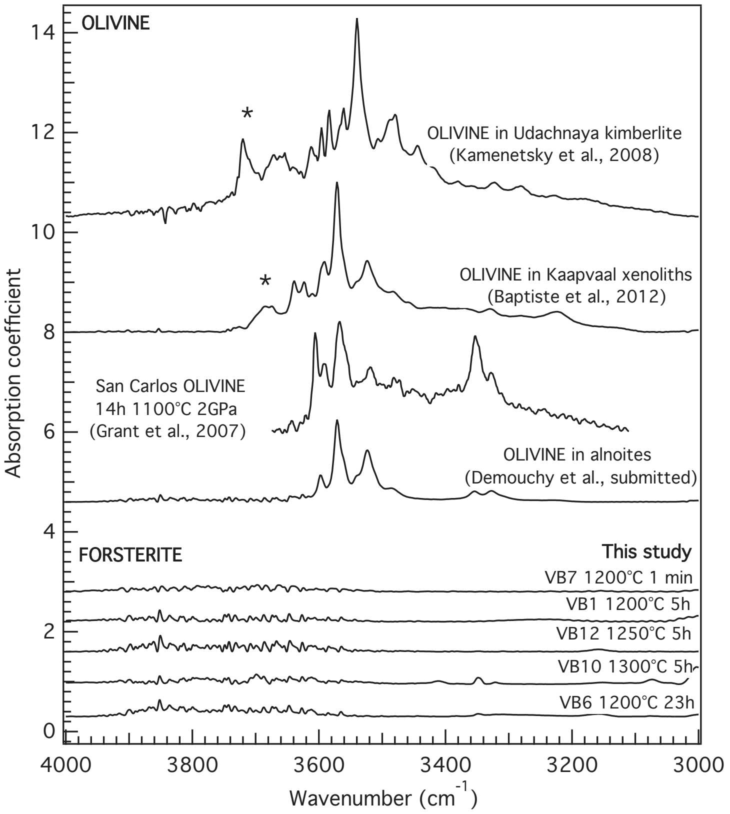

Figure 4: Unpolarized infrared spectra of the forsterite crystals after experiments (at 1 GPa) from this study. FTIR spectra from olivine in Udachnaya and Kaapvaal xenoliths (transported by kimberlite, Baptiste et al., 2012; Kamenetsky et al., 2008), in Malaita xenoliths (transported by alnoites, Demouchy et al. revised), and in San Carlos olivine hydrated after 14h in a piston-cylinder experiments at 1100°C and 2 GPa (Grant et al., 2007) are presented for comparison. All spectra are normalized to a sample thickness of 1 cm.

FTIR analyses were performed on the post-runs forsterite single crystal (center and border) as well as on the adjacent forsterite overgrowths. The unpolarized border spectra are displayed in Figures 4 and 5. For the same position in the forsterite single crystal, the FTIR spectra do not change as a function of temperature, or experimental duration (Figure 4) and display no OH bands within their absorption field in forsterite. Minor OH bands only appear after passing the interface between the forsterite single crystal and the forsterite overgrowths as shown in Figure 5. The amplitude of these bands increases with increasing distance from the interface. The OH absorption band located at 3698 cm^{-1} is the first to appear, and always exhibits the highest absorption coefficient. It can be attributed to serpentine or brucite (Miller et al., 1987). The minor band at 3612 cm^{-1} is characteristic of iron-free forsterite (Demouchy and Mackwell, 2003, Lemaire et al., 2004) and the large broad band at 3427 cm^{-1} was previously attributed to inter-granular water (e.g., Keppler and Rauch, 2000; Demouchy et al., 2012). In the next section, we discuss the lack of hydration of the forsterite single crystal and the possible consequences for the hydration state of the lithospheric mantle.

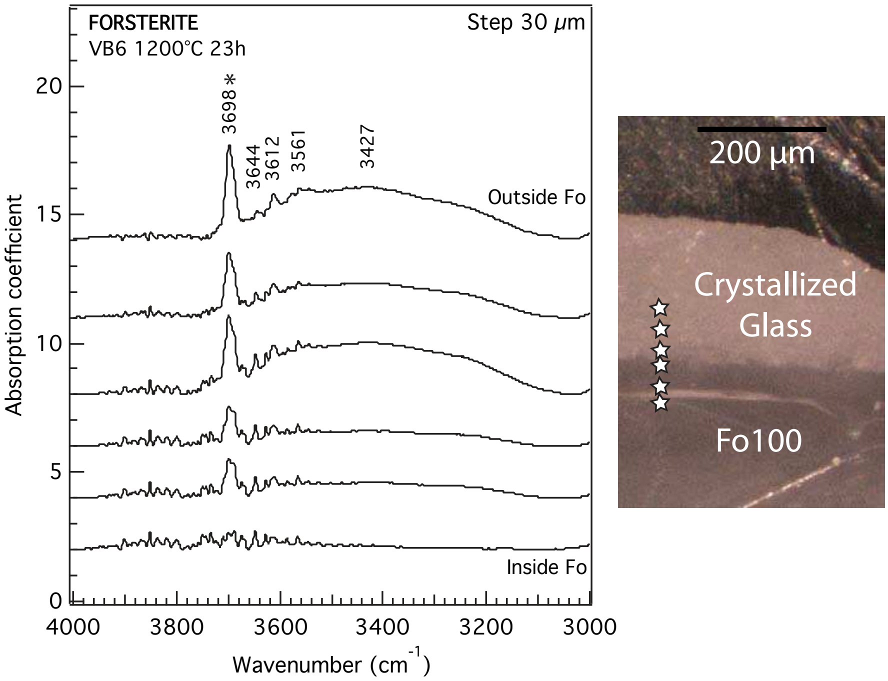

Figure 5: Unpolarized FTIR profile across the forsterite single crystal interface. Six spectra were measured with a step size of 30 μm. All spectra are normalized to a sample thickness of 1 cm. See text for OH band attribution.

Discussion

Unpolarized FTIR analyses has demonstrated that despite water-saturation of the system and long duration, none of forsterite single crystals display signs of hydration at OH saturation level or as diffusion profile of OH from the border toward the center of the crystal. Further, the absorption level of the FTIR spectra on the forsterite overgrowths does not even resemble the level of hydration from any of the characteristic spectra of mantle-derived or megacryst olivine transported by kimberlites from cratonic regions (Baptiste et al., 2012; Bell et al., 2004; Miller et al., 1987; Peslier et al., 2010) as shown in Figure 4. They also do not match the olivine or forsterite spectra from hydration experiments at high pressure and temperature in CO_2-free system for only few hours at temperature above 1100°C as previously reported (Demouchy and Mackwell, 2003; Grant et al., 2007; Lemaire et al., 2004; Sokol et al., 2013a, 2013b; Yang et al., 2014), except for the very weak bands at 3612 cm^{-1} and maybe that at 3361 cm^{-1}. The other, more intense, IR peaks present are linked to hydrous minerals (brucite and/or serpentine), and are most likely the result of the rapid pressure and temperature quench.

Theses experiments were set up to test if a volatile-rich kimberlitic liquid could hydrate mantle-derived olivine during their transport toward the surface. Hydration during transport could have explained the absence of dehydration profile in olivine crystals transported by kimberlite as well as the high water contents reported in mantle-derived olivine from cratonic setting if hydration took place at important depths (Baptiste et al, 2012; Bell et al. 2004; Doucet et al., 2014; Kamenetsky et al., 2007; Kurosawa et al., 1997; Miller et al. 1987). In all five experiments, no OH was found in the single crystal of forsterite, whatever the duration of the experiment. At 1 GPa and at water-saturated conditions in a CO_2-free system, OH content should reach 100 ppm H_2O wt in iron-bearing olivine (Kohlstedt et al., 1996; Férot and Bolfan-Casanova, 2012; Grant et al., 2007; Mosenfelder et al., 2006) and > 25 ppm H_2O wt in iron-free olivine (e.g., Demouchy and Mackwell, 2003; Lemaire et al., 2004; Grant et al., 2006; Bali et al., 2008). The run products reported here are far from such high hydrogen concentration. Further, it is known that in mixed fluids, composed of CO_2 and H_2O (Holloway and Blank, 1994), the fugacity of H_2O is reduced with the addition of CO_2, and vice-versa. Here, our simplest interpretation is that despite the high H_2O bulk content (>10 wt.%; Table 1) in the starting kimberlitic liquid, the presence of CO_2 has lowered the H_2O fugacity to such an extent that it has prohibited hydration of the forsterite single crystal or overgrowth (Figures. 4 and 5). The effect of CO_2 on lowering H_2O fugacity in kimberlitic liquids was previously anticipated by Sokol et al. (2013b) based on high-pressure, high-temperature crystallization experiments of olivine phenocrysts from a powder with a composition of an exotic erupted kimberlite (from Udachnaya, Siberia; Kamenetsky et al., 2008). Also, a recent experimental study from Yang et al., (2014) has assessed the effect of CO_2 on lowering H_2O fugacity in a melt-free system (i.e., hydrothermal annealing of natural olivine + free H_2O + $NaHCO_3$ or $Ag_2C_2O_4$). However, in this study, hydration was not completely inhibited and hydrogen incorporation was only reduced by a factor 2 under a pressure of 1.5-5 GPa. Thus, our results corroborate the results from Yang et al., (2014) and confirm the role of CO_2 in prohibiting significant hydration of the forsterite and olivine crystals.

The important forsterite overgrowth is a notable result from our experiments and was previously reported in hydration experiments (e.g., Kohlstedt et al., 1996; Bali et al., 2008). One may question the link between crystal overgrowth and the lack of hydration in our experiments. From over 20 measurements per crystallographic axis on the SEM images, we determine that the overgrowth length is in average after 5h at 1250°C: 72 µm parallel to [100] and 102 µm parallel to [001]; and after 23h at 1200°C: 179 µm parallel to [100] and 153 µm parallel to [001]). Two mechanisms of hydrogen diffusion can be considered based on two types of point defects in forsterite: hydrogen diffusion is rate limited by Mg-vacancy diffusivity or Si-vacancy diffusivity. Also, using the diffusion coefficients determined experimentally, one can calculate the characteristic distance (x) of hydrogen diffusion in forsterite (i.e., $x = 2 \times (Dt)^{1/2,}$ where D is the diffusion coefficient in m^2/s and t time in $s^{\cdot}$). Assuming a Mg-vacancy (Demouchy and Mackwell 2003, Padron-Navarta, et al., 2014), it yields after 5h at 1250°C a length of 263 µm parallel to [100] and 823 µm parallel to [001]; after 23h at 1200°C a length of 419 µm parallel to [100] and 1337 µm parallel to [001]. Therefore, if this mechanism of diffusion is assumed, the characteristic distance of hydrogen diffusion exceeds by far the overgrowth length and should have permitted the full hydration of the forsterite overgrowth and significant hydration of the forsterite single crystal. Assuming a Si vacancy-controlled diffusion of hydrogen (Padron-Navarta, et al., 2014) which is a slower mechanism of diffusion, it yields after 5h at 1250°C a length of 149 µm and after 23h at 1200°C a length of 174 µm. In this case, the characteristic distance is closed to the length of the overgrowth, therefore, even if the initial forsterite single crystal was not hydrated, the overgrowth should have incorporated significant H (>20 ppm H_2O wt). All available diffusion kinetics data and solubility experiments converge toward efficient hydrogen incorporation in a CO_2-free system. Except the drastic reduction of water fugacity favored in this study, the only remaining possibility to explain the lack of hydration would be an extremely slow diffusivity of hydrogen in the order of 1 to 5×10^{-15} m^2s^{-1} and accordingly, an unrealistic low vacancy concentration at such high temperature of annealing.

Furthermore, as regards to the lack of significant data on olivine grain growth, our crystallization experiments allow to estimate the rate of grain growth of forsterite crystals. In silicate systems with crystals and liquid at chemical equilibrium (with very small ΔT), Ostwald ripening (Ostwald, 1901) allows growth of large grains at the expense of the small ones and layer growth mechanism should control grain growth instead of continuous growth (Cabane et al., 2005). Following the relation linking grain size and time (e.g., Ardell, 1972; Kirkpatrick, 1975; Cabane et al., 2005) as:

$d^n - d_o^n = kt,$

where d and d_o are the final and initial grain size, n the grain growth exponent, k is the growth rate and t is time. For diffusion-control or spiral layer-growth control (i.e., screw dislocation based), it implies an exponent n equal to 3 (e.g., Cabane et al., 2005). For our experiment, at 1250 °C (VB12), it results in a growth rate of $k = 2.34 \times 10^8 \pm 0.90 \times 10^8$ $\mu m^3/h$ for the [100] axis and $2.28 \times 10^8 \pm 1.14 \times 10^8$ $\mu m^3/h$ for [001] axis. At 1200 °C (VB6), it yields a growth rate k of $1.34 \times 10^8 \pm 0.41 \times 10^8$ $\mu m^3/h$ for [100] axis and of $0.69 \times 10^8 \pm 0.29 \times 10^8$ $\mu m^3/h$ for [001] axis. Several studies on grain growth experiments in nano-scale monocrystalline aggregates (melt-free) reported generally slower forsterite (Fo_{100}) growth rates than in this study (with n equals to 4 for their case). Ohuchi and Nakamura (2007a, 2007b) obtained fast growth rates on dry and wet forsterite aggregates (2.29×10^4 and 6.31×10^3 $\mu m^4/h$, respectively) at similar pressure and temperature (1.2 GPa, 1200°C). At lower pressure and higher temperature (1-atm, 1380°C), Hiraga et al. (2010) measured slower growth rates (36 $\mu m^4/h$) from grain growth experiments on dry nano forsterite monomineralic aggregates (50 nm to 6 μm). Finally, grain growth experiments on dry nano forsterite plus 5%-enstatite aggregates conducted by Tasaka and Hiraga. (2013) at similar pressure and temperatures (1-atm, 1260-1380°C) resulted in growth rates (1.3-34.4 $\mu m^4/s$) of the same order of magnitude than Hiraga et al., (2010). In the olivine-basalt systems, based on the extrapolation from Cabane et al. (2005) and their experimental data, forsterite grain should grow of 5.79 and 9.45 μm after 5h and 23h, respectively. In our forsterite-kimberlite system, the forsterite single crystal growth more than ten times faster than the estimates from Cabane et al. (2005) for the same amount of time, emphasizing the potential role of volatiles (here CO_2 and H_2O) on the depolymerization of the melt and its effect on grain growth kinetics.

Implications

At the point defect scale, despite the simplified system under consideration, the results of this study emphasizes the complex interplay of volatiles (here CO_2 and H_2O) and their incorporation such as hydrogen in the crystalline lattice of nominally anhydrous minerals. The results point to the necessity to adjust with care the amount of the respective volatiles when quantification for ‘water capacity’ or ‘CO_2 capacity’ for the Deep Earth is attempted, since significant hydration (> 100 ppm H_2O wt) at pressure relevant of the lithospheric mantle (1-3 GPa) seems to take place in a CO_2-poor system only.

At larger scale, the main consequences from this experimental study is that the high OH concentrations measured in mantle-derived olivine from peridotites in cratonic settings must be representative of the mantle hydrogen concentration at depth (i.e., garnet stability field). They also seem to be unaffected by their transport in kimberlitic liquids from important depths. Therefore, the high OH concentrations measured in Kaapvaal craton xenoliths by Baptiste et al. (2012) were certainly acquired during their mantle history, and were likely to be controlled by metasomatism (Baptiste et al., 2012).

Acknowledgements

This study was financially supported by ANR JCJC “HyDeep” awarded to NBC. SK acknowledges partial support from the 7th framework CIG Marie-Curie EU grant (#303301).

References

Ackermand D., Seifert, F., Schreyer, W., (1975) Instability of sapphirine at high-pressure. Contributions to Mineralogy and Petrology, 50, 79-92.

Ardell, A.J. (1972) On the coarsening of grain boundary precipitates. Acta Metallurgica, 20, 601-609.

Bali, E., Bolfan-Casanova, N., Koga, K., (2008) Pressure and temperature dependence of H solubility in forsterite: an implication to water activity in the Earth interior. Earth Planet. Sci. Lett. 268, 354–363.

Baptiste, V., Tommasi, A., and Demouchy, S. (2012) Deformation and hydration of the lithospheric mantle beneath the Kaapvaal craton, South Africa. Lithos, 149, 31-50.

Becker, M., and Le Roex, A.P. (2006) Geochemistry of South African on- and off-craton, group I and group II kimberlites: Petrogenesis and source region evolution. Journal of Petrology, 47(4), 673-703.

Bell, D.R., Rossman, G.R., and Moore, R.O. (2004) Abundance and Partitioning of OH in a High-pressure Magmatic System: Megacrysts from the Monastery Kimberlite, South Africa. Journal of Petrology, 45(8), 1539-1564.

Bolfan-Casanova, N., Keppler, H., Rubie, D.C., 2000. Water partitioning between nominally anhydrous minerals in the MgO-SiO2-H2O system up to 24 GPa: Implications for the distribution of water in the Earth's mantle. Earth Planet. Sci. Lett. 182, 209–221.

Brooker, R.A., Sparks, R.S.J., Kavanagh, J.L., Field, M., (2011). The volatile content of hypabyssal kimberlite magmas: some constraints from experiments on natural rock compositions. Bull Volcanol 73, 959–981.

Buob, A., Luth, R.W., Schmidt, M.W., and Ulmer, P. (2006) Experiments on CaCO3-MgCO3 solid solutions at high pressure and temperature. American Mineralogist, 91(2-3), 435-440.

Cabane, H., Laporte, D., and Provost, A. (2005) An experimental study of Ostwald ripening of olivine and plagioclase in silicate melts: implications for the growth and size of crystals in magmas. Contributions to Mineralogy and Petrology, 150, 37-53.

Dalton, J.A., and Presnall, D.C. (1998) The continuum of primary carbonatitic kimberlitic melt compositions in equilibrium with lherzolite: Data from the system $CaO-MgO-Al_2O_3-SiO_2-CO_2$ at 6GPa. Journal of Petrology, 39(11-12), 1953-1964.

Deer, W.A., Howie, R.A., Zussman, J., 1992. An introduction to the Rock-forming minerals., 2nd ed. The Geological Society. London.

Demouchy S., Ishikawa A., Tommasi A., Alard, O. and Keshav S. Characterisation of the hydration in the oceanic mantle lithosphere: peridotite xenoliths from Ontong Java Plateau as an example. Revised for Lithos, September 2014.

Demouchy, S., and Mackwell, S.J. (2003) Water diffusion in synthetic iron-free forsterite. Physics and Chemistry of Minerals, 30, 786-794.

Demouchy, S., Mackwell, S., 2006. Mechanisms of hydrogen incorporation and diffusion in iron-bearing olivine. Phys. Chem. Minerals 33, 347–355.

Demouchy, S., Tommasi, A., Barou, F., Mainprice, D., and Cordier, P. (2012) Deformation of olivine in torsion under hydrous conditions. Physics of the Earth and Planetary Interiors, 202-203, 56-70.

Demouchy, S., Mainprice, D., Tommasi, A., Couvy, H., Barou, F., Frost, D.J., and Cordier, P. (2011) Forsterite to wadsleyite phase transformation under stress and consequences for the Earth's mantle transition zone. Physics of the Earth and Planetary Interiors, 184, 91-104.

Doucet, L.-S., Peslier, A.H., Ionov, D.A., Brandon, A.D., Golovin, A.V., Goncharov, A.G., and Ashchepkov, I.V. (2014) High water contents in the Siberian cratonic mantle linked to metasomatism: an FTIR study of Udachnaya peridotite xenoliths. Geochimica et Cosmochimica Acta, 137, 159-187.

Férot, A., and Bolfan-Casanova, N. (2012) Water storage capacity in olivine and pyroxene to 14 GPa: Implications for the water content of the Earth's upper mantle and nature of seismic discontinuities. Earth and Planetary Science Letters, 349-350, 218-230.

Gaetani, G.A., and Grove, T.L. (1998) The influence of water on melting of mantle peridotite. Contributions to Mineralogy and Petrology, 131, 323-346.

Grant, K., Ingrin, J., Lorand, J.P., Dumas, P., (2007). Water partitioning between mantle minerals from peridotite xenoliths. Contrib. Mineral. Petrol. 154, 15–34.

Grant, K., Kohn, S.C., Brooker, R.A., (2006). Solubility and partitioning of water in synthetic forsterite and enstatite in the system $MgO\text{-}SiO_2\text{-}H_2O$ +/- Al_2O_3. Contrib. Mineral. Petrol. 151, 651–664.

Gudfinnsson, G.H., and Presnall, D.C. (2005) Continuous gradations among primary carbonatitic, kimberlitic, melilitic, basaltic, picritic, and komatiitic melts in equilibrium with garnet lherzolite at 3-8 GPa. Journal of Petrology, 46(8), 1645-1659.

Hiraga, T., Tachibana, C., Ohashi, N., and Sano, S. (2010) Grain growth systematics for forsterite ± enstatite aggregates: Effect of lithology on grain size in the upper mantle. Earth and Planetary Science Letters, 291, 10-20.

Hirth, G., and Kohlstedt, D.L. (1996) Water in the oceanic upper mantle: Implications for rheology, melt extraction, and the evolution of the lithosphere. Earth and Planetary Science Letters, 144, 93-108.

Holloway, J.R., and Blank, J.G. (1994) Application of experimental results to C-O-H species in natural melts. In Mineralogical Society of America Reviews in Mineralogy, 30, 187-230.

Jacobsen, S.D., Jiang, F., Mao, Z., Duffy, T.S., Smyth, J.R., Holl, C.M., and Frost, D.J. (2008) Effects of hydration on the elastic properties of olivine. Geophys. Res. Lett., 35(14), L14303.

Kamenetsky, V.S., Kamenetsky, M.B., Sobole, A.V., Golovin, A.V., Demouchy, S., Faure, K., Sharygin, V.V., Kuzmin, D.V., (2008). Olivine in the Udachnaya-East Kimberlite (Yakutia, Russia): Types, compositions and origins. J. Petrol 49, 823–839.

Karato, S. (1990) The role of hydrogen in the electrical conductivity of the upper mantle. Nature, 347, 272-273.

Keppler, H. (2003) Water solubility in carbonatite melts. American Mineralogist, 88, 1822-1824.

Keppler, H., and Rauch, M. (2000) Water solubility in nominally anhydrous minerals measured by FTIR and HNMR. Physics and Chemistry of Minerals, 27, 371-376.

Kikuchi, S. (1928) Diffraction of cathode rays by mica. Japanese Journal of Physics, 5, 83-96.

Kirkpatrick, R.J. (1975) Crystal growth from the melt: A review. American Mineralogist, 60, 798-814.

Kjarsgaard, B.A., Pearson, D.G., Tappe, S., Nowell, G.M., and Dowall, D.P. (2009) Geochemistry of hypabyssal kimberlites from Lac de Gras, Canada: Comparisons to a global database and applications to the parent magma problem. Lithos, 112S, 236-248.

Kohlstedt, D.L., Keppler, H., and Rubie, D.C. (1996) Solubility of water in the alpha, beta, and Y phases of (Mg, Fe)2SiO4. Reviews in Mineralogy & Geochemistry, 123(4), 345-357.

Kurosawa, M., Yurimoto, H., and Sueno, S. (1997) Patterns in the hydrogen and trace element compositions of mantle olivines. Physics and Chemistry of Minerals, 24(6), 385-395.

Lemaire, C., Kohn, S.C., and Brooker, R. (2004) The effect of the silica activity on the incorporation mechanisms of water in synthetic forsterite: a polarized spectroscopic study. Contrib. Mineral. Petrol., 147, 48-57.

Mackwell, S.J., Kohlstedt, D.L., and Paterson, M.S. (1985) The role of water in the deformation of olivine single-crystals. Journal of Geophysical Research-Solid Earth and Planets, 90(NB13), 1319-1333.

Matsyuk, S.S., and Langer, K. (2004) Hydroxyl in olivines from mantle xenoliths in kimberlites of the Siberian platform. Contributions to Mineralogy and Petrology, 147(4), 413-437.

Matsyuk, S.S., Langer, K., and Hösch, A. (1998) Hydroxyl defects in garnets from mantle xenoliths in kimberlites of the Siberian platform. Contributions to Mineralogy and Petrology, 132(2), 163-179.

Matveev, S., and Stachel, T. (2007) FTIR spectroscopy of OH in olivine: A new tool in kimberlite exploration. Geochimica et Cosmochimica Acta, 71(22), 5528-5543.

Miller, G.H., Rossman, G.R., and Harlow, G.E. (1987) The natural occurrence of hydroxide in olivine. Physics and Chemistry of Minerals, 14(5), 461-472.

Mitchell, R.H. (1986) Kimberlites: Mineralogy, Geochemistry, and Petrology. 442 p. Plenum Press, New York.

Mitchell, R.H. (1995) Kimberlites, Orangeites, and Related Rocks. 410 p. Plenum Press, New York.

Mosenfelder, J.L., Deligne, N.I., Asimow, P.D., and rossman, G.R. (2006) Hydrogen incorporation in olivine from 2-12 GPa. Am. Min., 91, 285-294.

Ohuchi, T., and Nakamura, M. (2007a) Grain growth in the forsterite-diopside system. Physics of the Earth and Planetary Interiors, 160, 1-21.

Ohuchi, T., and Nakamura, M. (2007b) Grain growth in the system forsterite-diopside-water. Physics of the Earth and Planetary Interiors, 161, 281-304.

Ostwald, W. (1901) Uber die vemeintliche Isomerie des roten und gelben Quecksilberoxyds und die Oberflachen-spannung Fester Korper. Zeitschrift für Physikalische Chemie, 34, 495-512.

Padrón-Navarta, J.A., Hermann, J., and O'Neill, H. (2014) Site-specific hydrogen diffusion rates in Forsterite. Earth and Planetary Science Letters, 392, 100-112.

Paterson, M.S. (1982) The determination of hydroxyl by infrared absorption in quartz, silicate glasses and similar materials. Bulletin de Minéralogie, 105(1), 20-29.

Peslier, A.H. (2010) A review of water contents of nominally anhydrous natural minerals in the mantles of Earth, Mars and the Moon. Journal of Volcanology and Geothermal Research, 197(1-4), 239-258.

Peslier, A.H., Woodland, A.B., Bell, D.R., and Lazarov, M. (2010) Olivine water contents in the continental lithosphere and the longevity of cratons. Nature, 467, 78–81.

Smith, C.B., Allsopp, H.L., Kramers, J.D., Hutchison, G., and Roddick, J.C. (1985a) Emplacement ages of Jurassic-Cretaceous South African kimberlites by the Rb-Sr method on phlogopite and whole-rock samples. South African Journal of Geology, 88, 249-266.

Smith, C.B., Gurney, J.J., Skinner, E.M.W., Clement, C.R., and Ebrahim, N. (1985b) Geochemical character of Southern African kimberlites; a new approach based on isotopic constraints. South African Journal of Geology, 88(2), 267-280.

Sokol, A.G., Kupriyanov, I.N., and Palyanov, Y.N. (2013a) Partitioning of H_2O between olivine and carbonate-silicate melts at 6.3 GPa and 1400°C: Implications for kimberlite formation. Earth and Planetary Science Letters, 383, 58-67.

Sokol, A.G., Kupriyanov, I.N., Palyanov, Y.N., Kruk, A.N., and Sobolev, N.V. (2013b) Melting experiments on the Udachnaya kimberlite at 6.3-7.5GPa: Implications for the role of H_2O in magma generation and formation of hydrous olivine. Geochimica et Cosmochimica Acta, 101, 133-155.

Sparks, R.S.J., Brooker, R.A., Field, M., Kavanagh, J., Schumacher, J.C., Walter, M.J., and White, J. (2009) The nature of erupting kimberlite melts. Lithos, 112(1), 429-438.

Tasaka, M., and Hiraga, T. (2013) Influence of mineral fraction on the rheological properties of forsterite + enstatite during grain-size-sensitive creep: 1. Grain size and grain growth laws. Journal of geophysical Research: Solid Earth, 118, 1-21.

Xirouchakis, D., Hirschmann, M.M., and Simpson, F. (2001) The effect of titanium on the silica content and on mineral-liquid partitioning of mantle-equilibrated melts. Geochimica et Cosmochimica Acta, 65, 2201-2217.

Yang, X., Dingding, L., and Xia, Q. (2014) CO2-induced small water solubility in olivine and implications for properties of the shallow mantle. Earth and Planetary Science Letters, 403, 37-47.